

ESTIMATING CAMERA ROTATION PARAMETERS FROM A BLURRED IMAGE

Giacomo Boracchi^{a,b}, Vincenzo Caglioti^a, and Alberto Danese^a

^a*Dipartimento di Elettronica e Informazione,*

Politecnico di Milano, Via Ponzio, 34/5 20133 Milano

^b*Tampere International Center for Signal Processing,**

Tampere University of Technology, P.O. Box 553, 33101 Tampere, Finland.

giacomo.boracchi@polimi.it, vincenzo.caglioti@polimi.it, alberto.danese@mail.polimi.it

Keywords: Blurred Image Analysis, Camera Rotation, Camera Ego-motion, Blur Estimation, Space Variant Blur.

Abstract: A fast rotation of the camera during the image acquisition results in a blurred image, which typically shows curved smears. We propose a novel algorithm for estimating both the camera rotation axis and the camera angular speed from a single blurred image. The algorithm is based on local analysis of the blur smears. Contrary to the existing methods, we treat the more general case where the rotation axis can be not orthogonal to the image plane, taking into account the perspective effects that in such case affect the smears. The algorithm is validated in experiments with synthetic and real blurred images, providing accurate estimates.

1 INTRODUCTION

This paper concerns images corrupted by blur due to a camera rotation or to a rotating object in the scene. When the camera or the captured object are purely rotating, the image blur is determined by only two factors: the camera rotation axis a and its angular speed ω . We present a novel algorithm for estimating both a and ω , by analyzing the blur in a single image.

When the camera rotation axis and the angular speed are known, the rotationally blurred image can be restored by image coordinates transformation and blur inversion. In broad terms, the image is transformed from Cartesian to polar coordinates so that the blur becomes space invariant and can be inverted using a deconvolution based algorithm. Estimating correctly the camera rotation axis and its angular speed is therefore crucial for restoring these images as small errors in the polar transformation are amplified by blur inversion.

On the other hand, estimating a and ω from a single image can be also of interest for robotic application as these describe the camera ego-motion.

Figure 1 shows an image acquired during camera rotation. The shapes of the blur smears show that the



Figure 1: A rotationally blurred image.

blur is space variant. Typically, these are assumed arcs of circumferences, all having the same center. However, this approach neglects the perspective effects that occur when the rotation axis is not orthogonal to the image plane. The proposed algorithm estimates the camera rotation axis in the most general case when it is not necessarily orthogonal to the image plane. To the best of our knowledge this issue has never been correctly addressed before.

Besides the early works concerning rotational blur modeling and restoration, Hong and Zhang (Hong and Zhang, 2003) addressed the issue of both rotational blur estimation and removal. Their method is based on an image segmentation along circumferences to

*This work was partially supported by CIMO, the Finnish Centre for International Mobility (fellowship number TM-07-4952).

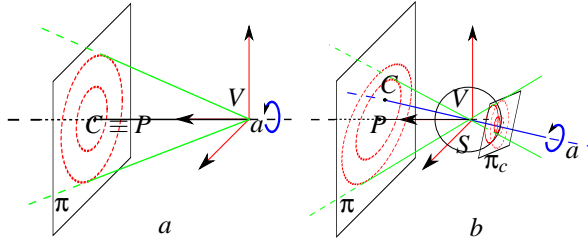


Figure 2: (a) Blurred image formation, $a \perp \pi$. Blurring paths are circumferences. (b) Blurred image formation, a is not orthogonal to image plane π and $V \in a$. Blurring paths are conic sections on the image plane, while they are circular when projected on an ideal spherical sensor and on a plane perpendicular to the rotation axis.

estimate the blur and restore the image separately in these subsets. Recently, an algorithm for estimating the camera rotation from a single blurred image has been proposed (Klein and Drummond, 2005). The algorithm is meant as a visual gyroscope and it is targeted to an efficient implementation. In particular, this algorithm requires edges in the scene.

All the existing methods, concerning both image restoration and blur estimation, assume that the blur smears are arcs of circumferences having the same center. Therefore these methods are accurate only on images where the rotation axis is orthogonal to the image plane.

We present an algorithm for estimating the camera rotation axis and angular speed in the most general case, where the rotation axis is not orthogonal to the image plane. The proposed algorithm is mostly targeted to accuracy rather than efficiency and does not require the presence of edges in the scene.

2 PROBLEM FORMULATION

We propose an algorithm for estimating the camera rotation axis a and its angular speed ω by analyzing a single blurred image acquired during camera rotation. We assume that the camera is calibrated, the rotation axis a passes through its viewpoint V , i.e. $V \in a$, and w is constant. Figure 2.a illustrates the situation typically considered in literature, where the rotation axis is perpendicular to image plane π . The principal point P and the intersection between the image plane and the rotation axis $C = \pi \cap a$ then coincide. Analogous blur is obtained when $a \perp \pi$ and $V \notin a$, but the capture scene is planar and parallel to π (Ribaric et al., 2000).

In this work we consider the most general situation, illustrated in Figure 2.b, where a is not orthogonal to π and the camera viewpoint $V \in a$.

2.1 Image Blur

A *blurring path* is defined as the set of image pixels that a viewing ray intersects during a camera rotation of 2π around axis a . Figure 2 illustrates examples of blurring paths. In rotationally blurred images every pixel is merged with neighboring pixels from the same blurring path, see Figure 1. The blur is therefore space variant and can not be represented as a linear shift invariant system. We therefore model the rotational blur by an operator K on the original image y (Bertero and Boccacci, 1998) so that the observed (blurred and noisy) image z is

$$z(\mathbf{x}) = K(y)(\mathbf{x}) + \eta(\mathbf{x}) \quad \mathbf{x} = (x_1, x_2) \in X, \quad (1)$$

\mathbf{x} being the coordinates in the discrete image domain X and $\eta \sim N(0, \sigma_\eta^2)$ is white Gaussian noise. The blur operator K can be written as

$$K(y)(\mathbf{x}) = \int_X k(\mathbf{x}, s)y(s)ds. \quad (2)$$

where $k(\mathbf{x}, \bullet)$ is a kernel

$$k(\mathbf{x}, \bullet) = A_{\theta, e}(\bullet), \quad (3)$$

and $A_{\theta, e}$ corresponds to the point spread function (PSF) at \mathbf{x} . $A_{\theta, e}$ being an arc the blurring path at \mathbf{x} , i.e. is an arc of conic section having tangent line with direction θ and arc length e . The parameters θ, e varies between image pixels according to the rotation axis a . Other blurring effects, such as the out of focus blur, lenses aberrations and camera shake, are not considered.

3 THE ALGORITHM

The proposed algorithm is based on three steps: in the first step the lines tangent to blurring paths at some image pixels are estimated (Section 3.1). In the second step, these lines are used in a voting procedure for estimating the rotation axis a (Sections 3.2 and 3.3). The third step consists of the angular speed ω estimation (Section 3.4).

3.1 Blur Tangent Direction Estimation

Image blur is analyzed within N image regions taken around selected pixels $\{\mathbf{x}_i\}_{i=1, \dots, N}$. There are no particular requirements in selecting $\{\mathbf{x}_i\}_{i=1, \dots, N}$, but avoiding smooth areas while covering uniformly the image. Therefore we take the local maxima of Harris corner measure (Harris and Stephens, 1988), or whenever these do not cover uniformly the image, we take $\{\mathbf{x}_i\}_{i=1, \dots, N}$ on a regular grid.

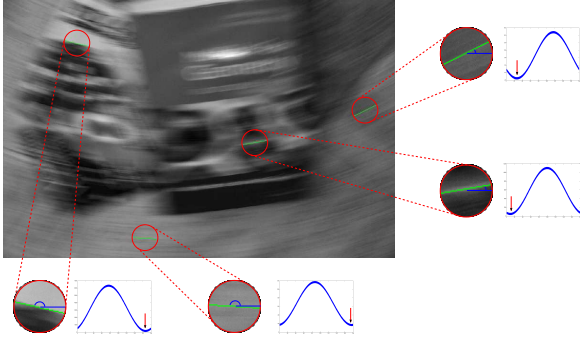


Figure 3: Rotationally blurred image and plots of directional derivatives energy in four regions.

Blur is analyzed using the approach proposed by Yitzhaky *et al* (Yitzhaky and Kopeika, 1996) for estimating the direction of blur “smears” by means of directional derivative filters. This method, proposed for space invariant blurs with PSF having vectorial support, assumes the image isotropic. The blur direction $\hat{\theta}$ is estimated as the direction of the derivative filter d_θ having minimum energy response

$$\hat{\theta} = \arg \min_{\theta \in [0, \pi]} (||d_\theta \otimes z||_1), \quad (4)$$

where \otimes denotes the convolution and $||d_\theta \otimes z||_1 = \sum_{\mathbf{x} \in X} |(d_\theta \otimes z)(\mathbf{x})|$ the ℓ^1 norm.

Equation (4) is motivated by the fact that the blur removes all the details and attenuates edges of y along blur direction. Therefore the blur direction can be determined by the directional derivative filter having minimum energy. This method can not be directly applied to rotationally blurred images, as the blur is not space invariant because in every pixel the circumference approximating the blurring path (i.e the PSF) changes.

At \mathbf{x}_i , the center of each region U_i , we estimate the direction θ_i of the line l_i tangent to the blurring path in \mathbf{x}_i , as

$$\theta_i = \arg \min_{\theta \in [0, \pi]} \sum_{\mathbf{x}_j \in U_i} w_j ((d_\theta \otimes z)(\mathbf{x}_j))^2. \quad (5)$$

being w a window function rotationally symmetric with respect to the center. By using Gaussian distributed weights, it is possible to reduce the influence of pixels in Equation (5) with the distance from \mathbf{x}_i . We adopted the 3 tap derivative filters presented in (Farid and Simoncelli, 2004) for blur analysis in Equation (5). These filters have been selected as they provide good accuracy and as they are separable. Experimentally the ℓ^2 norm gave better results than the ℓ^1 norm.

Figures 3 shows $\sum_{\mathbf{x}_j \in U_i} w_j ((d_\theta \otimes z)(\mathbf{x}_j))^2$ as a function of $\theta \in [0, \pi]$ within regions of the blurred image containing isotropic textures or edges. Regions

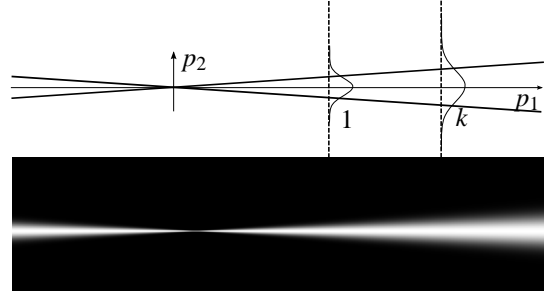


Figure 4: Weight function used for the votes spread.

containing edges, as pointed out in (Klein and Drummond, 2005), can be exploited for estimating the camera rotation: in z only edges tangent to the blurring paths are preserved. Formula (5) gives accurate results also when U_i contains a blurred edge, as the direction minimizing the derivatives energy is the edge direction, i.e the blur tangent direction.

3.2 Voting Procedure for Circular Blurring Paths

When the camera optical axis and the rotation axis a coincide, the blurring paths are circumferences centered in $C = \pi \cap a$, see Figure 2.a. Circular blurring paths are obtained also when a is parallel to the optical axis and the scene is planar and parallel to the image plane (Ribaric *et al.*, 2000; Hong and Zhang, 2003). In this case C can be determined by a Generalized Hough Transform (Ballard, 1987).

The Generalized Hough Transform is a procedure for computing robust solution to a problem, given some input data. The procedure is developed by means of a parameters space P , which is the set of all the possible solutions. A vote is assigned to every parameter that satisfy a datum and then summed to the votes coming from the other data. After having considered all the data, the parameter that received the highest vote is taken as a solution.

In our case P is a discrete grid of all the possible location for $C \in \pi$ and data are the pairs $(\mathbf{x}_i, \theta_i) \quad i = 1, \dots, N$. Note that C could be outside of the image grid X . Every data (\mathbf{x}_i, θ_i) identifies a line l_i , the line tangent to the blurring path at \mathbf{x}_i . The set of all the possible rotation centers C , given the line l_i , is the line perpendicular to l_i and passing through \mathbf{x}_i .

It is worth to take into account the root mean square error of each θ_i i.e.

$$\sigma_i = \sqrt{E[(\theta_i - \theta_i^*)^2]} \quad (6)$$

where θ_i^* represents the true tangent blur direction at \mathbf{x}_i and $E[\bullet]$ the mathematical expectation. Since

we can not directly compute σ_i , we approximate it with an indirect measurement: for example considering the amplitude of the area near θ_i in the energy function minimized in (5) or considering σ_i proportional to σ_η (1). Noise standard deviation is estimated using (Donoho and Johnstone, 1994). Given a datum (\mathbf{x}_i, θ_i) , we assign a full vote to all the exact solutions and we spread smaller votes to the neighboring parameters, according to the errors in θ_i .

Let now $\mathbf{p} = (p_1, p_2)$ represent a coordinate system in the parameters space and assume $\theta_i = 0$ and $\mathbf{x}_i = \mathbf{p}_i = (0, 0)$. Let now model the vote spread assuming that along the line $p_1 = 1$ the errors are distributed as $\sigma_i \sqrt{2\pi} \cdot N(0, \sigma_i)$. We model the vote spread so that along line $p_1 = k$, the votes are still Gaussian distributed with a full vote at the exact solution $(k, 0)$ and for neighboring parameters the votes depend only on the angular distance from θ_i , see Figure 4. Therefore the following weight function is used for distributing the votes in the parameter space (when $\mathbf{x}_i = \mathbf{p}_i = (0, 0)$ and $\theta_i = 0$),

$$v_i(p_1, p_2) = e^{-\frac{p_2^2}{1+p_1^2\sigma_i^2}}, \quad (7)$$

The votes weight function v_i , associated to other data (x_i, θ_i) , correspond to Equation (7) opportunely rotated and translated. When all pairs (x_i, θ_i) $i = 1, \dots, N$ have been considered, the parameter that received the highest vote is taken as the solution, i.e.

$$\hat{\mathbf{p}} = \arg \max_{\mathbf{p} \in P} \mathcal{V}(\mathbf{p}), \quad \text{being} \quad \mathcal{V}(\mathbf{p}) = \sum_{i=1}^N v_i(\mathbf{p}). \quad (8)$$

The coordinates of $C = \pi \cap a$ are determined from $\hat{\mathbf{p}}$.

3.3 Conic Section Blurring Paths

Assuming circular blurring paths reduces the complexity load but gives inaccurate solutions whenever a is not perpendicular to π . We present an algorithm for estimating a and ω when $V \in a$ and a is in a general position w.r.t. π . In particular, if we call π_C a plane perpendicular to a , π_C is obtained by two rotations of α and β from π . We do not consider $V \notin a$ as in this case the blur would depend on the scene depth.

Votes in the parameters space show at a glance what happens assuming circular blurring paths when a is not orthogonal to π . Figure 5.a shows a blurred image produced when the plane orthogonal to a forms angles $\alpha^* = 45^\circ$ and $\beta^* = 0^\circ$ with π . If we treat the blurring paths as circumferences, the votes in the parameters space do not point out a clear solution, as shown in Figure 5.b and 5.c.

Directions θ_i obtained from (5) represent the blurring paths tangent direction, even when the blurring

paths are conic sections. But the blurring paths themselves are not circumferences, thus lines perpendicular to these tangent lines do not cross at the same point.

From basic 3D geometry considerations, and as pointed out in (Klein and Drummond, 2005), it follows that the blurring paths are circumferences on an ideal spherical sensor S , Figure 2.b. Then, if we project the image from π on S surface, the blurring paths become circumferences. Each of these circumferences belongs to a plane and all these planes have the same normal: the rotation axis a . Let now consider one of these planes, π_C , tangent to the sphere. The projections of the blurring paths on π_C are circumferences, Figure 2.b.

The plane π and the plane π_C are related by a projective transformation determined by two parameters, namely (α, β) , the angles between the two planes. Define the map $M_{\alpha, \beta} : \pi \mapsto \pi_{\alpha, \beta}$ as the projection from V between π and $\pi_{\alpha, \beta}$, which is the plane tangent to S , forming angles (α, β) with π (Rothwell et al., 1992). We search for (α, β) that project the blurring paths into circumferences, by modifying the voting procedure of Section 3.2.

There is no need to transform the whole image with $M_{\alpha, \beta}$ as each l_i , the line tangent to the blurring path at \mathbf{x}_i , can be directly mapped via $M_{\alpha, \beta}$. Let $v_i^{\alpha, \beta}$ be the weight function (7) associated to data (\mathbf{x}_i, θ_i) $i = 1, \dots, N$ mapped via $M_{\alpha, \beta}$. The parameters pair identifying the plane π_C is estimated as

$$(\hat{\alpha}, \hat{\beta}) = \arg \max_{\alpha, \beta} \mathcal{V}^{\alpha, \beta}(\hat{\mathbf{p}}_{\alpha, \beta}), \quad (9)$$

being

$$\hat{\mathbf{p}}_{\alpha, \beta} = \arg \max_{\mathbf{p} \in P} \mathcal{V}^{\alpha, \beta}(\mathbf{p}), \quad \mathcal{V}^{\alpha, \beta}(\mathbf{p}) = \sum_{i=1}^N v_i^{\alpha, \beta}(\mathbf{p}). \quad (10)$$

Figure 5.d and 5.e represent the votes in case the data have been transformed according to the correctly estimated parameters $\hat{\alpha} = 45^\circ, \hat{\beta} = 0^\circ$. These votes are much more concentrated than votes in Figure 5.b and 5.c.

Once $\hat{\alpha}$ and $\hat{\beta}$ have been estimated, the camera rotation axis a is determined and it is possible to map the image z to $M_{\hat{\alpha}, \hat{\beta}}(z)$. As said before, in $M_{\hat{\alpha}, \hat{\beta}}(z)$ the blurring paths are circumferences centered at $M_{\hat{\alpha}, \hat{\beta}}(C) \equiv \pi_C \cap a$ and it is therefore possible to transform $M_{\hat{\alpha}, \hat{\beta}}(z)$ in polar coordinates for estimating the angular speed.

3.4 Angular Speed Estimation

Once C has been determined, it is possible to transform $M_{\hat{\alpha}, \hat{\beta}}(z)$ (the image projected on π_C) on a polar

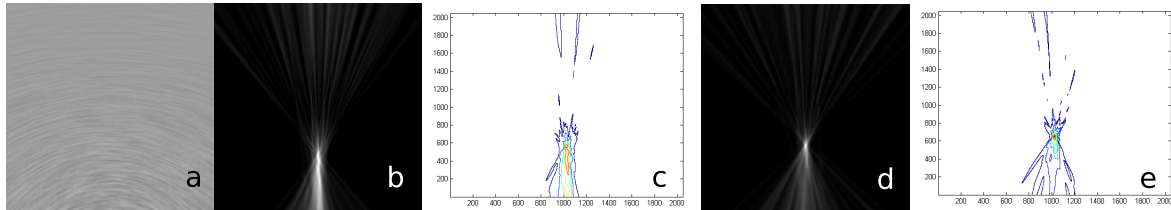


Figure 5: (a) Rotationally blurred image with rotation axis $\alpha^* = 45^\circ, \beta^* = 0^\circ$. (b) Votes assuming circular blurring paths, (c) votes contours. (d) Votes obtained transforming the data with $\hat{\alpha} = 45^\circ, \hat{\beta} = 0^\circ$, (e) votes contours. The maximum vote in (d) is 33% higher than the maximum vote in (b). This is due to the fact that transforming the data with $M_{45,0}$ the blurring paths become circumferences having the same center.



Figure 6: Still and rotationally blurred synthetic images. First row, left to right: Boat ($\alpha^* = 20^\circ, \beta^* = 0^\circ$), Mandrill ($\alpha^* = -20^\circ, \beta^* = 20^\circ$) and Lena ($\alpha^* = 0^\circ, \beta^* = -20^\circ$). Second row: Boat, Mandrill and Lena, rotationally blurred with an angular speed of 6, 8 and 6 deg/s, respectively, assuming 1 second of exposure time. Intersection between image plane and rotation axis is marked with a red circle.

lattice (ρ, θ) w.r.t to $M_{\hat{\alpha}, \hat{\beta}}(C)$ (Ribaric et al., 2000). On the polar lattice, the blur is space invariant with the PSF directed along lines $\rho = const$. We estimate the PSF extent using the method proposed by Yitzhaky (Yitzhaky and Kopeika, 1996) as this can be applied to a restricted image area, avoiding lines which contain several pixels of padding introduced by the polar transformation. The PSF extent, opportunely scaled by the factor due to the polar lattice resolution, divided by the exposure time gives the camera angular speed.

4 EXPERIMENTS

The algorithm has been validated both on synthetic and camera images. Synthetic images of Figure 6 have been generated with a raytracer software (<http://www.povray.org/>), rotating the camera in front

Table 1: Boat. Highest votes corresponding to (α, β) in the parameters space, expressed as a percentage with respect to the maximum vote.

α	β	-40	-20	0	20	40
-40		33	52	72	53	48
-20		39	52	83	63	44
0		34	57	83	63	43
20		40	55	100	55	44
40		35	42	62	39	34

Table 2: Refinement around $(\hat{\alpha}, \hat{\beta})$ from Table 1.

α	β	-10	0	10
10		71	79	80
20		63	100	74
30		57	82	61

of planar tiles of test images. Blurred images are obtained averaging all the rendered frames, according to Equation (1). Ten frames (512x512 pixels, grayscale 0-255) are rendered per each rotation degree. The blurring paths tangent directions are estimated in 121 equally spaced regions having a 10 pixel radius, using formula (5).

Table 1 shows $\mathcal{V}^{\alpha, \beta}(\hat{\mathbf{p}}_{\alpha, \beta})$ (the value of the maximum vote obtained with (α, β)) as a percentage w.r.t $\mathcal{V}^{\hat{\alpha}, \hat{\beta}}(\hat{\mathbf{p}}_{\hat{\alpha}, \hat{\beta}})$ (the maximum vote obtained with $(\hat{\alpha}, \hat{\beta})$). Here $(\hat{\alpha}, \hat{\beta})$ coincides with (α^*, β^*) , the ground truth. Table 2 shows the results at a second iteration considering a refinement around $(\hat{\alpha}, \hat{\beta})$.

Table 3 shows results obtained on synthetic images of Figure 6. Each of them has been tested adding white gaussian noise with standard deviation 0, 0.5 and 1 and considering α and β in $A = B = \{-40^\circ, -20^\circ, 0^\circ, 20^\circ, 40^\circ\}$. Algorithm performances are evaluated with $\Delta(\alpha) = |\hat{\alpha} - \alpha^*|$ and $\Delta(\beta) = |\hat{\beta} - \beta^*|$. $\Delta(\hat{C})$ and $\Delta(\hat{\omega})$ represent the absolute error between the ground truth and the estimated values of $C = \pi \cap a$ and ω , respectively.

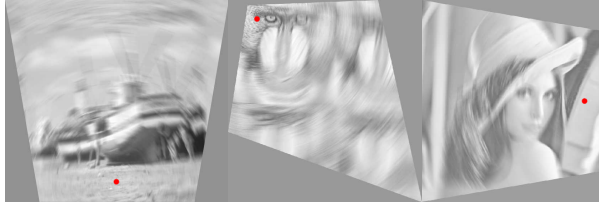


Figure 7: Boat, Mandrill and Lena rectified with the corresponding estimated $(\hat{\alpha}, \hat{\beta})$. Intersection between the image plane and the rotation axis is marked with a red circle.

The effectiveness of our algorithm is evaluated as

$$adv = \frac{\mathcal{V}^{\hat{\alpha}, \hat{\beta}}(\hat{\mathbf{p}}_{\hat{\alpha}, \hat{\beta}}) - \mathcal{V}^{\alpha_2, \beta_2}(\hat{\mathbf{p}}_{\alpha_2, \beta_2})}{\mathcal{V}^{\alpha_2, \beta_2}(\hat{\mathbf{p}}_{\alpha_2, \beta_2})}, \quad (11)$$

being $\mathcal{V}^{\alpha_2, \beta_2}(\hat{\mathbf{p}}_{\alpha_2, \beta_2})$ the maximum vote obtained among other parameters (α, β) . The higher this ratio, the better. Finally, $\Delta(C^{0,0})$ and $\Delta(\omega^{0,0})$ are the corresponding errors obtained assuming circular blurring paths. Results for noisy images represent the average over ten different noise realizations.

Results reported in Table 3 show that our algorithm can cope with a reasonable amount of noise, obtaining regularly better results than the circular blur assumption. This is more evident in the estimation of the angular speed, which lacks physical meaning when the rotation axis is not correctly identified. Figure 7 shows blurred images of Figure 6 transformed with the corresponding $M_{\hat{\alpha}, \hat{\beta}}$.

Camera images have been captured rotating a Canon EOS 400D camera on a tripod, assuring that a is orthogonal to the floor. The ground truth α^* and β^* , can be then computed rectifying still images of a checkerboard on the floor. Figures 8.a and 10.a show the downsampled RAW converted in grayscale used to test our algorithm. The blurring path tangent directions are estimated on 187 uniformly spaced regions, having 10 pixel radius.

Tables 4 and 5 show the results of the execution of two iterations of the algorithm on Figure 8.a. The solution obtained is $\hat{\alpha} = -30^\circ$ and $\hat{\beta} = 0^\circ$, which is acceptable as the ground truth, obtained from the checkerboard, is $(-27^\circ, 0^\circ)$. Figure 9 points out the differences between the blurring paths estimated with the circular approximation (in red) and the conic section paths estimated by our method (in green). As clearly seen from the detail, the blur is correctly interpreted by the green blurring paths. Figure 10 shows results on another camera image, having $\alpha^* = -20^\circ$ and $\beta^* = 0^\circ$. After two iterations, the algorithm converges exactly to the correct solution. Figures 8 and 10 show the blurred images and the checkerboard images rectified with the estimated $(\hat{\alpha}, \hat{\beta})$.

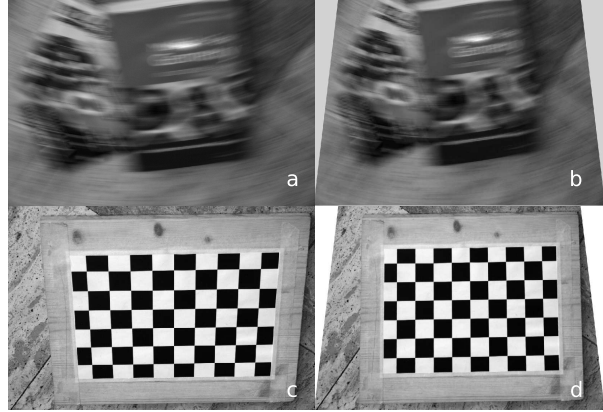


Figure 8: Blurred camera image. (a) Blurred image ($\alpha^* = -27^\circ, \beta^* = 0^\circ$), (b) rectified image with estimated $\hat{\alpha} = -30^\circ, \hat{\beta} = 0^\circ$, (c) checkerboard with the same camera inclination, (d) checkerboard rectified with $\hat{\alpha} = -30^\circ, \hat{\beta} = 0^\circ$.

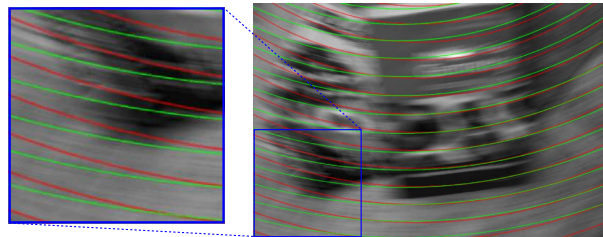


Figure 9: Comparison between circular (red) and conic section (green) blurring paths on 8.a. Green blurring paths describe more accurately the image blur.

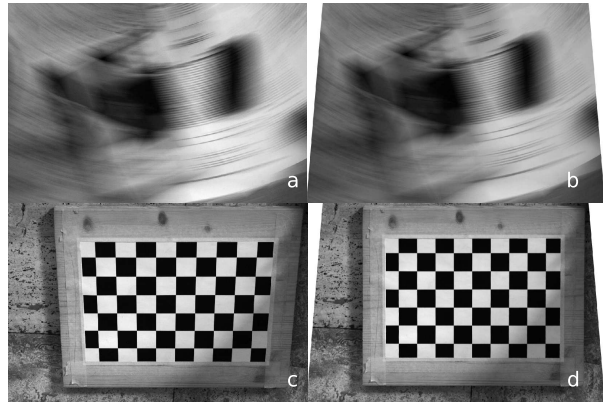


Figure 10: Blurred camera image. (a) Blurred image ($\alpha^* = -20^\circ, \beta^* = 0^\circ$), (b) rectified image with estimated $\hat{\alpha} = -20^\circ, \hat{\beta} = 0^\circ$, (c) checkerboard with the same camera inclination, (d) checkerboard rectified with $\hat{\alpha} = -20^\circ, \hat{\beta} = 0^\circ$.

5 CONCLUSIONS

We described a novel algorithm for estimating the camera rotation axis and the angular speed from a sin-

Table 3: Algorithm performances on synthetic images. When $\sigma_\eta > 0$, averages over 10 noise realizations.

Image	σ_η	$\Delta(\alpha)$	$\Delta(\beta)$	$\Delta(\hat{C})$	$\Delta(\hat{\omega})$	$adv(\%)$	$\Delta(C^{0,0})$	$\Delta(\omega^{0,0})$
Boat	0	0	0	2.20	0.23	20.44	33.06	4.83
Boat	0.5	0	0	5.46	0.24	20.23	21.27	114.55
Boat	1	0	0	8.84	0.19	8.84	19.25	71.98
Mandrill	0	0	0	1.00	0.09	5.66	7.07	0.96
Mandrill	0.5	2	2	1.48	0.11	6.13	4.81	2.85
Mandrill	1	4	4	1.17	0.26	5.25	4.41	2.29
Lena	0	0	0	3.00	0.08	11.01	12.08	0.60
Lena	0.5	0	0	3.88	0.20	14.06	33.64	64.94
Lena	1	0	4	5.23	0.48	6.00	29.43	62.58

Table 4: Camera Image. Highest votes corresponding to (α, β) in the parameters space, expressed as a percentage with respect to the maximum vote.

α	β	-40	-20	0	20	40
-40		63	88	100	88	52
-20		62	77	78	70	54
0		67	74	80	70	62
20		62	81	85	65	63
40		71	73	82	78	77

Table 5: Camera Image. Refinement around $(\hat{\alpha}, \hat{\beta})$ from Table 4.

α	β	-10	0	10
-50		82	76	80
-40		81	96	72
-30		85	100	83

gle blurred image. The algorithm provides accurate estimates also in the most challenging cases, when the rotation axis is not orthogonal to the image plane. To the best of the authors' knowledge, none of the existing methods handles these cases correctly since said methods assume circular blurring paths. We have shown how this assumption produces inaccurate estimates when the rotation axis is not orthogonal to the image plane, while our algorithm is more accurate.

The algorithm is targeted to accuracy rather than efficiency. Accuracy in the estimation of these parameters is a primary issue in restoring such images as the deblurring is typically based on a coordinate transformation and a deconvolution, which are highly sensitive to errors.

Ongoing works concern the design of a more noise-robust method for blur analysis on image regions and the implementation of a faster voting procedure.

REFERENCES

- Ballard, D. H. (1987). Generalizing the hough transform to detect arbitrary shapes. In *Readings in Computer Vision: Issues, Problems, Principles, and Paradigms*, pages 714–725. Morgan Kaufmann Publishers Inc., San Francisco, CA, USA.
- Bertero, M. and Boccacci, P. (1998). *Introduction to Inverse Problems in Imaging*. Institute of Physics Publishing.
- Donoho, D. L. and Johnstone, I. M. (1994). Ideal spatial adaptation by wavelet shrinkage. *Biometrika*, 81(3):425–455.
- Farid, H. and Simoncelli, E. (2004). Differentiation of discrete multi-dimensional signals. *IEEE Transactions on Image Processing*, 13(4):496–508.
- Harris, C. and Stephens, M. (1988). A combined corner and edge detector. In *Proceedings of the 4th Alvey Vision Conference*, pages 147–151.
- Hong, H. and Zhang, T. (2003). Fast restoration approach for rotational motion blurred image based on deconvolution along the blurring paths. *Optical Engineering*, 42:347–3486.
- <http://www.povray.org/>.
- Klein, G. and Drummond, T. (2005). A single-frame visual gyroscope. In *Proc. British Machine Vision Conference (BMVC'05)*, volume 2, pages 529–538, Oxford. BMVA.
- Ribaric, S., Milani, M., and Kalafatic, Z. (2000). Restoration of images blurred by circular motion. In *Image and Signal Processing and Analysis, 2000. IWISPA 2000. Proceedings of the First International Workshop on*, pages 53–60.
- Rothwell, C., Zisserman, A., Marinos, C., Forsyth, D., and Mundy, J. (1992). Relative motion and pose from arbitrary plane curves. *IVC*, 10:250–262.
- Yitzhaky, Y. and Kopeika, N. S. (1996). Identification of blur parameters from motion-blurred images. In Tescher, A. G., editor, *Proc. SPIE Vol. 2847, p. 270-280, Applications of Digital Image Processing XIX, Andrew G. Tescher; Ed.*, pages 270–280.